NANO LETTERS

pubs.acs.org/NanoLett Letter

Interfacial Resistive Switching by Multiphase Polarization in Ion-Intercalation Nanofilms

Huanhuan Tian and Martin Z. Bazant*

Cite This: https://doi.org/10.1021/acs.nanolett.2c01765 Read Online

ACCESS | Metrics & More | Article Recommendations | Supporting Information

ABSTRACT: Nonvolatile resistive-switching (RS) memories promise to revolutionize hardware architectures with in-memory computing. Recently, ion-interclation materials have attracted increasing attention as potential RS materials for their ion-modulated electronic conductivity. In this Letter, we propose RS by multiphase polarization (MP) of ion-intercalated thin films between ion-blocking electrodes, in which interfacial phase separation triggered by an applied voltage switches the electron-transfer resistance. We develop an electrochemical phase-field model for simulations of coupled ion-electron transport and ion-modulated electron-transfer rates and use it to analyze the MP switching current and time, resistance ratio, and current−voltage response. The model is able to reproduce the complex cyclic voltammograms of lithium titanate (LTO) memristors, which cannot be explained by existing models based on bulk dielectric breakdown. The theory predicts the achievable switching speeds for multiphase ion-intercalation materials and could be used to guide the design of high-performance MP-based RS memories.

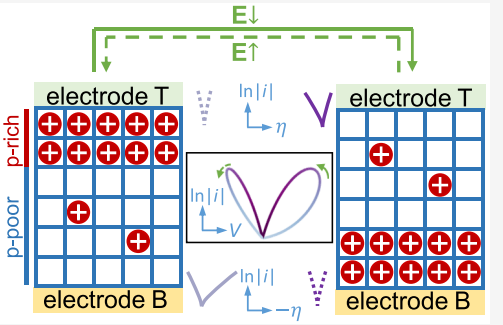

KEYWORDS: *resistive switching, phase-field modeling, electron transfer, ion intercalation*

In the era of Big Data, the transfer of data between the processing unit and memory has increasingly limited the performance of traditional computing architectures. The "von Neumann bottleneck" can potentially be addressed by in-memory computing, which requires resistive-switching (RS) devices with multiple, nonvolatile resistance states that can be tuned by applied voltages.[1−6] RS devices include two-terminal memristors and three-terminal synaptic transistors.[5] The switching can be bipolar or unipolar, depending on whether the set and reset voltages require different signs, respectively.[4] Studied RS mechanisms include ion migration,[1,3,7−11] amorphouscrystalline transition,[3,10−13] ferroelectricity,[3,10] and tunneling magneto-resistance.[3,10] This work describes an RS mechanism based on interfacial phase separation that is limited by bulk ion migration.

Typically, the ion migration mechanism incorporates an ion-conducting nanofilm and an active electrode that can inject (consume) active ions or vacancies into (from) the nanofilm. Specifically, the mechanism is called electrochemical metallization (ECM) if metal cations (e.g., Cu^{2+}, Ag^{+}) are active and valence change mechanism (VCM) if oxygen vacancies are active.[1,5] The ion migration mechanism can be further divided into the bulk and interfacial types, according to which resistance dominates. The bulk mechanisms often involve the formation of conductive filaments (e.g., Cu, Ag, or oxygen vacancy rich regions) by implantation of ions or vacancies from an active electrode, and the dissolution of the filaments by a reverse process driven by a reverse voltage (bipolar switching) or by Joule heating generated by a larger voltage (unipolar switching).[8−11,14] In the interfacial mechanisms, usually the two electrodes have, respectively, ohmic contact and Schottky contact with the nanofilm, and the latter is sensitive to the local concentration of ions or vacancies which can be enriched or depleted by electric field (bipolar switching).[7,11,15−18]

In recent years, ion-intercalation materials, which have been widely used for batteries,[19−21] have received increasing attention as novel ion-migration-based RS materials. These materials allow for reversible insertion of ions into the lattice without destroying the original crystal structure,[22] often following a multiphase mechanism.[23] Their electronic conductivity usually depends on ion concentration, since the inserted/deserted ions usually contribute (nearly) free electrons/holes to the conduction/valence bands.[24−28] This property has been directly used to design bulk-type memristors[29] and synaptic transistors[26,30−32] for which the ion concentration is adjusted by ion insertion/desertion through the active or gate electrodes. Compared to ECM or VCM devices, such devices should have good reproducibility and controllability since the conductivity can be precisely and reversibly controlled by current pulses.[26]

Received: May 1, 2022
Revised: July 2, 2022

https://doi.org/10.1021/acs.nanolett.2c01765
Nano Lett. XXXX, XXX, XXX−XXX

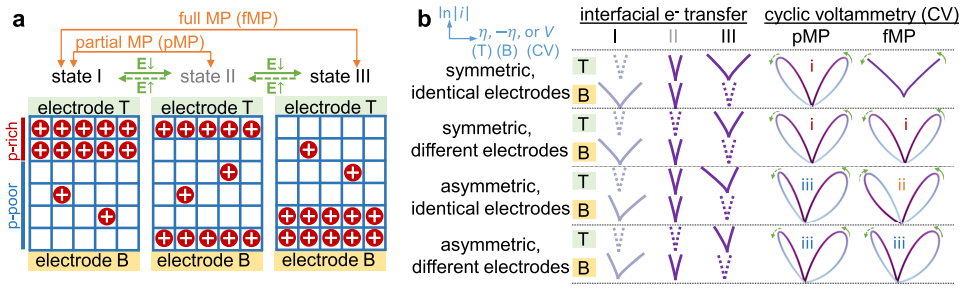

Figure 1. (a) Schematics of the phase redistribution (state I ↔ II ↔ III) by applied electric field (**E**, for which the direction is ↑or ↓) between ion-blocking electrodes, a process which we refer to as multiphase polarization (MP). (b) Effect of MP on interfacial electron transfer (ET) rates and the resulting total resistance switching characterized by cyclic voltammetry, for different combinations of electrodes. We call an electrode symmetric if it does not conduct current primarily in one direction and two electrodes identical if they have the same ET rates given the same local concentration and overpotential. The two electrodes can be different due to materials and deposition conditions. Each electrode contact is assumed to be more conductive and symmetric at higher concentrations. Each curve represents the log of current ($\ln|i|$) vs interfacial overpotential η or $-\eta$ for the top (T) or bottom (B) electrode at steady state or vs the applied voltage V for cyclic voltammetry. The ET rates shown by solid curves dominate total resistance. Three patterns of cyclic voltammetry are identified: (i) symmetric pattern with separated states, (ii) symmetric pattern with crossed states, and (iii) asymmetric patterns.

This work focuses on ion-intercalation memristors enclosed by ion-blocking electrodes, inspired by the LTO (lithium titanate, $Li_{4+3\xi}Ti_5O_{12}$) memristors developed in ref 33. LTO is a commonly used anode material for Li-ion batteries, and follows a two-phase mechanism and insulator−metal transition during lithiation (ξ: 0 → 1).[34] The memristors were made of LTO4 ($\xi \approx 0$) or LTO7 nanofilms ($\xi \approx 1$) sandwiched by Pt electrodes and showed bipolar switching behaviors. The ion-blocking electrodes make the RS mechanism different from those reviewed before. References 33 and 35 explain the RS of LTO memristors by the formation of conductive filaments by dielectric breakdown, based on a phase-field model including the electrostatic self-energy that depends on the magnitude of the applied potential. However, the RS predicted by this model is either volatile or irreversible, since the filaments should quickly dissolve after removing the voltage or never dissolve even with a reverse voltage (see the Supporting Information (SI)).

In this Letter, we propose a new nonvolatile and reversible interfacial RS mechanism, multiphase polarization (MP), fo LTO memristors and other similar systems made of multi-phase, ion-intercalation nanofilms enclosed by ion-blocking electrodes.

MECHANISM

We begin by noting the following properties of LTO memristors derived from experimental data: (1) interfacial ET should dominate the total resistance, since the effective conductivity of LTO4 and LTO7 measured by electrochemical impedance spectroscopy in ref 33 is around 2×10^{-11} and 6×10^{-10} S/m, respectively, at 30 °C, which are small compared with the bulk values in the literature: 10^{-4}−10^{-11} and 1−10^{2} S/m;[34,36,37] (2) the two electrodes should have different ET resistance due to different deposition temperatures; (3) LTO4 and LTO7 may not be pure (only Raman spectroscopy was used to estimate Li concentration) and both phases may exist in each memristor; (4) the ET rates usually strongly depend on local ion concentrations.[23,38]

These complex properties, which are not captured by existing theories, motivate us to propose the general MP mechanism, illustrated in Figure 1. We assume that the nanofilm conducts cations and electrons while the electrodes only conduct electrons. Then cations tend to move along the electric field but get blocked by the electrodes. Therefore, cations accumulate downstream the electric field and get depleted on the other side. This phenomenon is called concentration polarization (CP) and is important in many electrochemical systems.[39−50] In multiphase materials, CP should first occur in each phase and strong enough CP can change the phase distribution, which we refer to as multiphase polarization (MP). As shown in Figure 1a, a downward electric field may drive phase change at the bottom electrode first (I → II) and then at the bottom electrode later (II → III). We call the processes I ↔ II partial MP (pMP) and I ↔ III full MP (fMP). The phase distribution should be nonvolatile after removing the applied voltages, since phases with different concentration can coexist in multiphase materials, unlike CP in homogeneous electrolytes. The phase distribution can further influence ET rates on electrodes and thus significantly influence the total resistance if it is dominated by contact resistance, as shown in Figure 1b. For example, if the two electrodes are symmetric (do not conduct electrons primarily in one direction) but the top electrode is more conductive than the bottom electrode given the same concentration and overpotential, then state I should have larger total resistance than state III, and thus fMP can lead to RS.

To conclude, MP is an interfacial RS mechanism, limited by bulk ion diffusion, which shows multiple, nonvolatile resistance states tunable by applied voltages in LTO memristors and other similar systems.

MODEL

Here, we develop an electrochemical phase-field model to quantitatively describe the mechanism, based on nonequilibrium thermodynamics of ion and electron transfer.[23] We neglect temperature variation which should be mild for the interfacial RS mechanism without hot filaments (see the SI), and we neglect mechanical effects for "zero-strain" LTO.[34] Existing phase-field models of ion-intercalation mater ials in Li-ion batteries[23,51−60] and memristors[35] consider only the dynamics of neural Li^+-electron pairs. However, here we must account for large electric fields and broken symmetry between ion and electron transfer at the electrode interfaces. As such, our model includes three charged species: mobile, localized electrons ("n"), mobile, monovalent cations ("p"), and fixed, positively charged defects ("d"). The localized

https://doi.org/10.1021/acs.nanolett.2c01765
Nano Lett. XXXX, XXX, XXX−XXX

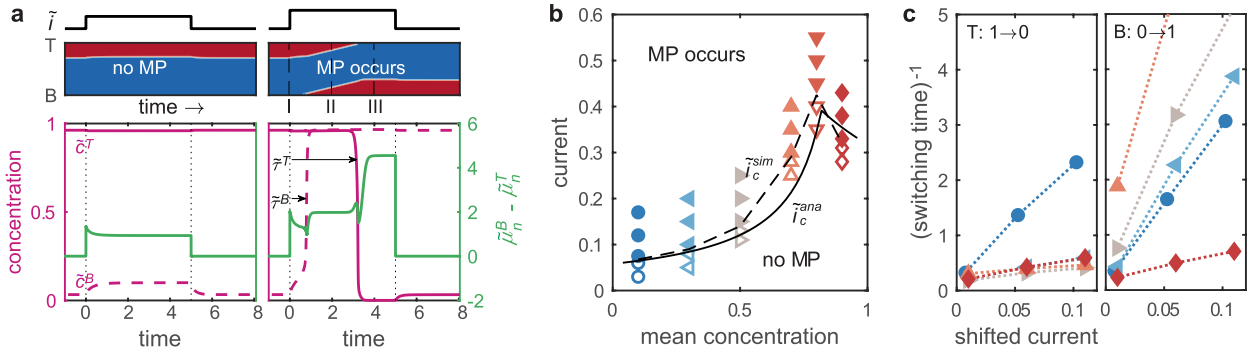

Figure 2. Switching current and switching time from simulations of step current response. (a) From top to bottom: applied current ($\tilde{i} = i/i_D$), phase distribution (contour map: red, ion-rich phase 1; blue, ion-poor phase 0), boundary concentrations ($\tilde{c}^T$, $\tilde{c}^B$), electrochemical potential drop ($\tilde{\mu}_n^B - \tilde{\mu}_n^T$), along with time ($\tilde{t} = t/\tau_D$) for two typical cases (with mean concentration $\tilde{c}_m = 0.3$, current plateau $\tilde{i}_{max} = 0.08, 0.12$). The schematics for the three typical states I, II, and III during MP can be found in Figure 1. The switching time $\tilde{\tau}$ can be obtained from $\tilde{\tau}^T = \tilde{t}_{\tilde{c}^T=0.5}$ and $\tilde{\tau}^B = \tilde{t}_{\tilde{c}^B=0.5}$. (b) Critical current ($\tilde{i}_c$) for MP to occur indicated by simulations (filled and empty markers to indicate MP and no MP, dashed line for eye guidance) and theory (solid line) for different mean concentrations ($\tilde{c}_m$). (c) Inverse of the switching time ($1/\tilde{\tau}$) along with the shifted current ($\tilde{i} - \tilde{i}_c^{ana}$). The colors and markers to label concentrations in (b,c) are consistent.

mobile electrons, also called "small polarons" for their coupling with the polarized local environment (including nearby mobile ions), differ from band electrons by a much smaller but thermally activated mobility and a nonthermally activated number of mobile electrons. Such electrons are often found in mixed-valency transition metal oxides,[28,61−64] which include some of the most common ion-intercalation materials used in Li-ion batteries and other applications.[65] The fundamental constants we use include the Boltzmann constant k_B, temperature T, electron charge e, thermal voltage $V_T = k_BT/e$, and the Avogadro number N_A. We denote the concentration, valence, electrochemical potential, diffusivity, conductivity, and flux density of mobile species k (=p, n) as c_k, z_k (=±1), μ_k, D_k, σ_k, and $\mathbf{J}_k$, and the electric potential, current density, time, and nanofilm thickness as ϕ, i, t, and h. We also define dimensionless variables $\tilde{c}_k = c_k/c_0$,$\tilde{\mu}_k = \mu_k/k_BT$, $\tilde{\phi} = \phi/V_T$, $\tilde{t} = t/\tau_D = tD_p^0/h_2$, $\tilde{J}_k = \mathbf{J}_k h/D_k^0 c_0$, and $\tilde{i} = i/i_D = i/(D_n^0 c_0 N_A e/h)$, where c_0 and D_k^0 are constants.

First, we enforce electroneutrality:

$$\tilde{c}_p = \tilde{c}_n - \tilde{c}_d = \tilde{c} \tag{1}$$

Then, we apply a regular solution model with Cahn−Hillard gradient expansion for the two charge carriers (k = p, n):[23,63,66−69]

$$\tilde{\mu}_k = \ln \frac{\tilde{c}_k}{\tilde{c}_k^{max} - \tilde{c}_k} + \tilde{\mu}_k^0 + \Omega_k \tilde{c}^\rho + z_k\tilde{\phi} - \kappa_k \tilde{\nabla}^2 \tilde{c} \tag{2}$$

where the five terms are ideal entropy for a mixture of charge carriers and vacancies on c_k^{max} sites, constant standard energy, mixing enthalpy, electrostatic potential energy, and Cahn−Hillard gradient penalty with $\kappa_n = \kappa_p = \kappa$. Next, we can use the homogeneous part of $\tilde{\mu}_p + \tilde{\mu}_n$ (with $\Omega = \Omega_n + \Omega_p$ defined) to determine the thermal stability (see the SI), including the spinodal points $\tilde{c}_{s0}$, $\tilde{c}_{s1}$ and the binodal points $\tilde{c}_{b0}$, $\tilde{c}_{b1}$ (0, ion-poor phase; 1, ion-rich phase). Compared with recent models of Li-ion battery materials,[35,51,59,60,70] this analysis includes the electrochemical potential of electrons and uses an additional parameter "ρ" to adjust concentration-symmetry in the Gibbs free energy of mixing.

Next, we describe the transport of charge carriers by enforcing mass and charge conservation with the generalized Nernst−Planck equation for charge fluxes[23,71]

$$r_k \frac{\partial \tilde{c}_k}{\partial \tilde{t}} + \tilde{\nabla}\cdot\tilde{\mathbf{J}}_k = 0, \quad \mathbf{J}_k = -D_k c_k \nabla \tilde{\mu}_k \tag{3}$$

where $\tilde{\nabla} = h\nabla$, $r_p = 1$, and $r_n = D_p^0/D_n^0$. The diffusivity with the excluded volume effects is $D_k = D_k^0(1 - c_k/c_k^{max})$, and the corresponding ionic/electronic conductivity is $\sigma_k = D_k c_k e N_A/V_T$. We neglect field-dependence of D_k,[72] since we assume most of the electric potential falls at interfaces. The boundary conditions on the electrodes with outward normal vector $\mathbf{n}$ are no penetration of ions $\mathbf{n}\cdot\tilde{\mathbf{J}}_p = 0$, conservation of electrons $\mathbf{n}\cdot\tilde{\mathbf{J}}_n = -\mathbf{n}\cdot\tilde{\mathbf{i}}$, and neutral wetting $\mathbf{n}\cdot\tilde{\nabla}\tilde{c} = 0$.

Finally, and critically, we must describe the ion-modulated ET rates at electrode interfaces. At metal−semiconductor interfaces, the ET rates can be described by diffusion, tunneling, or thermoemission across a Schottky barrier, which can be significantly influenced by doping ions.[38,73,74] However, unlike band conduction in traditional semiconductors, this work focuses on small polaron conduction in mixed-valency intercalation materials. In another words, the bulk ET in LTO and interfacial ET at the LTO−Pt interface can be described by $Ti^{4+} + Ti^{3+} \rightleftharpoons Ti^{3+} + Ti^{4+}$ and $Ti^{4+} + e^-(Pt) \rightleftharpoons Ti^{3+}$, respectively. This ET mechanism, though in solids, is very analogous to the ET reactions in liquid solutions and at liquid−solid interfaces as described by Marcus theory,[64,75] which involves a microscopic picture of solvent fluctuation and predicts curved Tafel plots (log current vs voltage) at large overpotentials as observed in experiments.[76−81] Recently, Marcus theory was also applied to solid-state ET in carbon-coated lithium iron phosphate.[75] However, the original Marcus theory and the asymmetric Marcus theory which has very limited applicability[82−84] cannot capture the significant asymmetry possibly seen at solid−solid interfaces. Then we notice the facts that Marcus theory reduces to the phenomenological Butler−Volmer (BV) equation at small to medium overpotentials[23,81,85,86] and the BV equation with a series resistance can also lead to curved Tafel plots.[51] Though usually used for ion transfer, the BV equation can be used for general Faraday reactions[23] including $Ti^{4+} + e^-$ (Pt) $\rightleftharpoons Ti^{3+}$. Actually, a Schottky diode is also usually described by a BV-form formula in combination with a series resistance to fit the curved Tafel plots,[38,87,88] though the ion-modulated exchange current should be different from the system we study here. As a first approximation to capture these diverse phenomena, we

https://doi.org/10.1021/acs.nanolett.2c01765
Nano Lett. XXXX, XXX, XXX−XXX

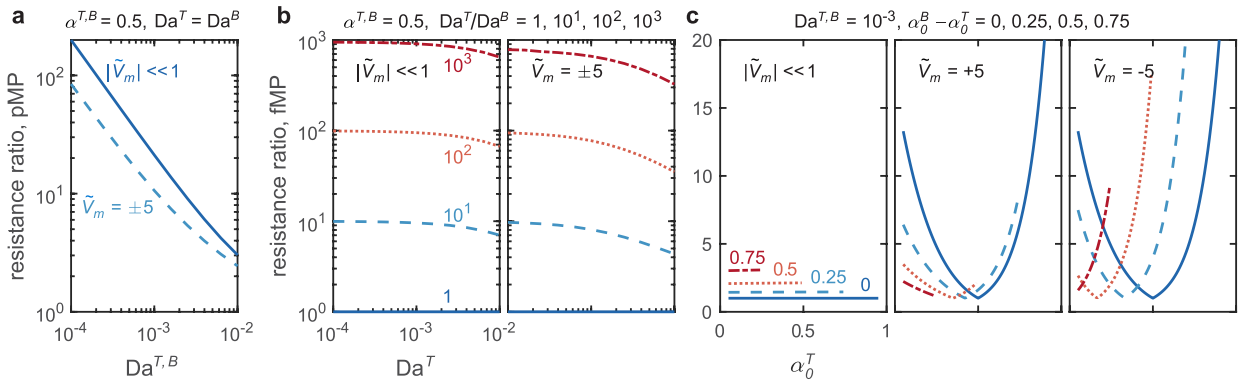

Figure 3. Resistance ratio ($\mathcal{R}$) measured at different voltages ($\tilde{V}_m = V_m/V_T$) due to (a) pMP and identical, symmetric electrodes and (b) fMP and symmetric electrodes with various rate constants Da, (c) fMP and asymmetric electrodes with the same Da. For pMP, $\mathcal{R} = \exp\left(\left|\ln \frac{\tilde{R}(\tilde{c}_{b1}, \tilde{c}_{b0})}{\tilde{R}(\tilde{c}_{b1}, \tilde{c}_{b1})}\right|\right)$. For fMP, $\mathcal{R} = \exp\left(\left|\ln \frac{\tilde{R}(\tilde{c}_{b1}, \tilde{c}_{b0})}{\tilde{R}(\tilde{c}_{b0}, \tilde{c}_{b1})}\right|\right)$. Here we choose $\tilde{c}_m = 0.5$ to calculate the bulk resistance.

propose the following generalized BV equation, which includes nonideal thermodynamics to capture the concentration dependence and a series resistance $\tilde{R}_s$ to serve a similar role as Marcus theory to curve the Tafel plots:[23,51]

$$\mathbf{n}\cdot\tilde{\mathbf{i}} = \mathrm{Da} f(\tilde{c};\alpha) g(\tilde{\eta};\alpha) e^{-\alpha\kappa\tilde{\nabla}^2\tilde{c}} \tag{4a}$$

$$f(\tilde{c};\alpha) = (\tilde{c}_n/\tilde{c}_n^{\max})^{\alpha}(1-\tilde{c}_n/\tilde{c}_n^{\max})^{1-\alpha}\, e^{\alpha\Omega_n\tilde{c}^{\rho}} \tag{4b}$$

$$g(\tilde{\eta};\alpha) = e^{(1-\alpha)\tilde{\eta}} - e^{-\alpha\tilde{\eta}} \tag{4c}$$

where $\tilde{\eta} = \tilde{\mu}_n - \tilde{\mu}_e$ is the overpotential across the interface, $\tilde{\mu}_e = \tilde{\mu}_e^0 - \tilde{\phi}_e$ is the Fermi energy in the electrode, and $\tilde{\phi}_e^B = 0$, $\tilde{\phi}_e^T = \tilde{V} - \tilde{I}\tilde{R}_s$ (where $\tilde{I}$ is the total current and in 1D $\tilde{I} = \tilde{i} = \tilde{\mathbf{i}}\cdot\mathbf{e}_x$, $\tilde{V}$ is the applied voltage, "T" and "B" represent the two electrodes at top and bottom). We further assume $\alpha = \alpha_0 + (0.5 - \alpha_0)\tilde{c}$ so that ET asymmetry disappears for large $\tilde{c}$ (ohmic contact). Constants Da and α^0 can be different for the two electrodes. See the SI for the derivation of eq 4.

DIMENSIONLESS RESULTS

We proceed to use our model to analyze RS performance of multiphase ion-intercalation nanofilms[4] in terms of dimensionless variables. As an example to test the model, we choose parameters based on the LTO material[24,34,36,37,71,89,90] (see the SI): $\tilde{c}_p^{\max} = 1$, $\tilde{c}_n^{\max} = 5/3$, $\Omega = -12$, $\rho = 0.7$, $\kappa = 1.1 \times 10^{-3}$, $\Omega_n = 20$, $D_p/D_n = 10^{-5}$, $\tilde{c}_d = 0.01$, and $\tilde{R}_s = 100$. Note that these values are all obtained/estimated from the experiments in the literature without fitting and especially $\tilde{R}_s$ is estimated from the reorganization energy of the small polarons.

We first analyze switching current and time, based on 1D simulations of MP in response to a step current (no need to consider ET here) as shown in Figure 2. Figure 2a shows two typical cases. Both cases reach steady state during the applied current, but only the larger current causes MP, in which case the time scale ($\tilde{\tau}^T$, $\tilde{\tau}^B$) for phase change at the two electrodes can be determined. The smaller one of $\tilde{\tau}^T$, $\tilde{\tau}^B$ is the time for pMP to occur, while the larger one is for fMP to occur. Then the switching current and time for more cases with different averaged concentration $\tilde{c}_m$ and applied current $\tilde{i}$ are summarized in Figure 2b,c. The condition under which MP occurs can be explained as follows. In each phase, the concentration rises at the downstream of the electric field and falls on the other side. If this perturbation in either phase is large enough to cause phase change, MP occurs. We also derive an approximate, analytical expression for the critical current:

$$\tilde{i}_c^{\mathrm{ana}} = \min\left\{\frac{\mathcal{F}|_{\tilde{c}_{b0}}^{\tilde{c}_{s0}}}{\tilde{h}_0(\tilde{c}_m)}, \frac{\mathcal{F}|_{\tilde{c}_{s1}}^{\tilde{c}_{b1}}}{1-\tilde{h}_0(\tilde{c}_m)}\right\} \tag{5}$$

where $\mathcal{F}(\tilde{c})$ is the effective potential for current ($\tilde{i} = \tilde{\nabla}_x\mathcal{F}$) and $\tilde{h}_0(\tilde{c})$ is an estimate of the occupation of the ion-poor phase 0 (see the SI). This expression is consistent with simulations, as shown in Figure 2b. For the switching time, we find that its reciprocal is roughly proportional to the current, as shown in Figure 2c. We also find that the end concentrations ($\tilde{c} = 0.1, 0.9$) have similar switching times on the two sides, in which cases pMP is unlikely to be observed. And the $\tilde{c} = 0.1$ case switches faster than $\tilde{c} = 0.9$. At medium concentrations, there is a big time window between pMP and fMP, which makes it possible to utilize pMP for RS.

Next, we analyze the resistance ratio (measured by voltage $\tilde{V}_m$) for different combinations of interfacial ET parameters. Here we consider steady state and assume $|\tilde{V}_m|$ is not large enough to significantly perturb the bulk concentration profiles. If $|\tilde{V}_m| \ll 1$, the total resistance is $\tilde{R}(\tilde{c}^T, \tilde{c}^B) = \frac{1}{\mathrm{Da}^T f(\tilde{c}^T;\alpha^T)} + \frac{1}{\mathrm{Da}^B f(\tilde{c}^B;\alpha^B)} + \tilde{R}_b + \tilde{R}_s$, where $\tilde{R}_b$ is the bulk resistance and is usually much smaller than the other resistances (see the SI). If $|\tilde{V}_m| > 1$, we need to solve $\tilde{R}$ from the current balance. Then we can compare $\tilde{R}$ for different states and calculate the resistance ratio $\mathcal{R}$ (≥ 1 by definition), as shown in Figure 3. First, we need to know when MP can lead to RS ($\mathcal{R} > 1$). Basically, for symmetric, identical electrodes, only pMP can lead to RS (see Figure 3a and the $Da^T/Da^B = 1$ case in Figure 3b). For other cases, fMP can also lead to RS. Then, to get a larger $\mathcal{R}$, the ET on the two electrodes should dominate the total resistance and be very different after MP. Therefore, larger Ω_n (more Fermi energy lift due to ion intercalation) is preferred. In addition, for symmetric electrodes, $\mathcal{R}$ should decrease for larger Da, smaller Da ratios, larger $|\tilde{V}_m|$, as shown in Figure 3a,b. For asymmetric electrodes, the situation is more complex. Both the magnitude and sign of $\tilde{V}_m$ are very important, as shown in Figure 3c. Only large enough $|\tilde{V}_m|$ can lead to $\mathcal{R} > 1$ for identical, asymmetric electrodes and fMP (solid lines). Moreover, $\mathcal{R}$ for asymmetric, different electrodes depends on the sign of $\tilde{V}_m$.

https://doi.org/10.1021/acs.nanolett.2c01765
Nano Lett. XXXX, XXX, XXX−XXX

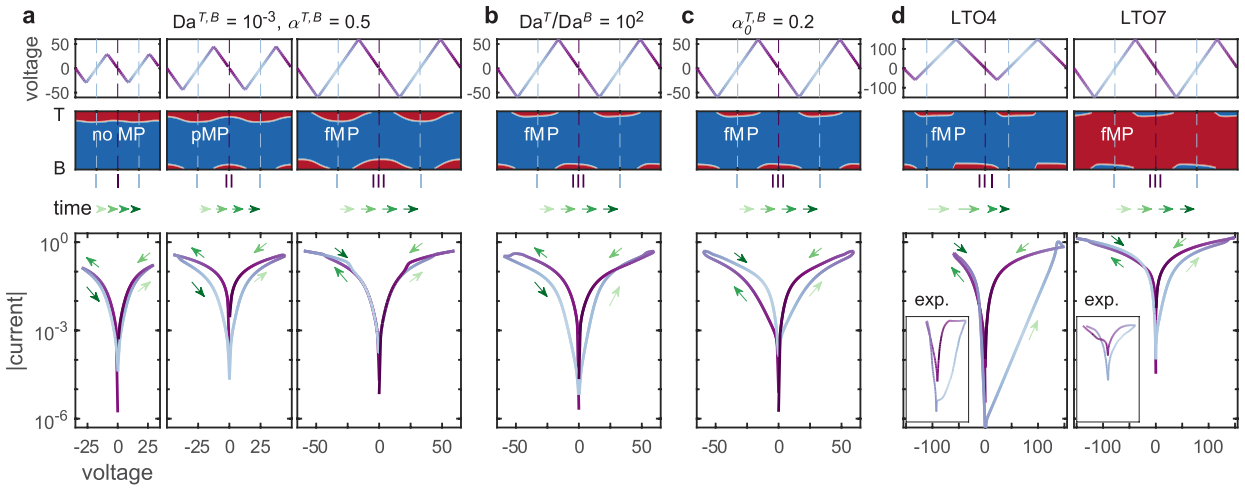

Figure 4. Simulation results of cyclic voltammetry for two cycles. From top to bottom: applied voltage ($\tilde{V} = V/V_T$) versus time ($\tilde{t} = t/\tau_D$), phase distribution (red, ion-rich phase 1; blue, ion-poor phase 0) versus time ($\tilde{t}$), and current ($|\tilde{i}| = |i/i_D|$) versus voltage ($\tilde{V}$). The sweeping rate is 125 at a dimensionless scale, or 50 mV/s if the diffusion time $\tau_D = 64$ s. Four sets of electrodes are considered: (a) identical, symmetric electrodes with three maximum sweeping voltages, (b) symmetric, different electrodes, (c) identical, asymmetric electrodes, and (d) different, asymmetric electrodes to fit for experiments of LTO4 and LTO7 memristors from ref 33. The dashed lines in the time evolution figures label three typical states, and schematics for states I, II, and III can be found in Figure 1. Interfacial parameters not shown in the figure: (b) $Da^T = 10^{-2}$, (c) $Da^{T,B} = 10^{-3}$, (d) LTO4: $Da^T = 10^{-3}$, $Da^B = 10^{-6}$, $\alpha_0^T = 0.3$, $\alpha_0^B = 0.08$, LTO7: $Da^T = 10^{-1}$, $Da^B = 10^{-3}$, $\alpha_0^T = 0.05$, $\alpha_0^B = 0.2$. Mean concentration: $\tilde{c}_m = 0.2$, 0.1, 0.1, 0.1, and 0.9 for (a), (b), (c), (d) LTO4, and (d) LTO7, respectively.

Finally, we analyze the cyclic voltammetry behaviors. As expected (Figure 1), for symmetric and identical electrodes, only pMP can lead to RS, as shown in Figure 4a. A Da ratio and fMP can lead to separated states (Figure 4b), while asymmetric α and fMP can lead to crossed states (Figure 4c), around zero voltage.

COMPARISON WITH EXPERIMENTS

For dimensional analysis, we use additional parameters: $c_0 = 22$ M, $h = 80$ nm, electrode area $S = 500\ \mu m \times 500\ \mu m$, and $D_p^0 = 1 \times 10^{-16}$ m^2/s (see the SI). The theory works well for the LTO memristors[33] in terms of the following three aspects.

First, the theory predicts that the switching time is limited by the ion diffusion time ($\tau_D = 64$ s), though it can be reduced by over 10 times by increasing the current (Figure 2). Therefore, we predict switching time in seconds, which is consistent with experiments.

Second, without any fitting parameters, our theory indicates that the LTO4 memrsitor should have faster switching than LTO7 and need less current (case $\tilde{c} = 0.1$, 0.9 in Figure 2), which is also consistent with Figure 2c,d in ref 33.

Finally, by choosing proper interfacial parameters, we can obtain cyclic voltammetry patterns similar to experiments (Figure 2a,b in ref 33), as shown in Figure 4d. Note that the dimensionless current at low and high voltage is mainly determined by Da and $\tilde{R}_s$, respectively, and the dimensional current scale is mainly determined by the diffusion current i_D. Since electronic conductivity can vary by magnitudes due to defects,[36,37] we may assume LTO7 conductivity to be ~0.005 S/m to quantitatively fit the experimental current in Figure 4d (see the SI).

However, the 1D simple picture cannot predict the numerous resistance states and finite retention time observed in experiments. These issues may be explained by 2D or 3D phase nucleation, which may also reduce the switching current significantly.

DISCUSSION AND PERSPECTIVES

Our model provides some fresh insights into the optimization and possible alternative designs for MP-based memristors.

First, the switching time of existing LTO memristors (on the order of seconds) is too long for the requirements of in-memory computing, including neuromorphic artificial synapses ($\lesssim\mu$s−ms)[91] and digital computing ($\lesssim$ns).[3] The performance can be improved by changing from LTO to intercalation materials with high ion mobility, decreasing nanofilm thickness, or increasing current. For example, we can choose intercalation materials with lower-dimensional diffusion paths (Figure 5a), e.g., nanosized LFP (defects-sensitive 1D paths),[92] layered materials (2D paths)[21] like MoS_2,[93−95] LCO,[96] graphite,[19,97] and even 2D materials (with only a few layers).[20,98] The ion diffusivity for these examples are shown in Figure 5b. Note that these intercalation materials all have phase separation and strong concentration dependence of conductance (thus usually of contact resistance), which is necessary for MP-induced RS. We then assume the nanofilm thickness is 50 nm and the switching time is 1/10 of the diffusion time, and put the axes for diffusion and switching time in Figure 5b. This is a conservative estimation, but note that we need a thick enough nanofilm to allow coexistence of different phases, and a too large current may lead to problems like Li plating. As we can see, we should be able to obtain switching time of μs−ms which is sufficient for neuromorphic computing.

In addition, the theory implicitly indicates infinite retention time, without state decay by diffusion which usually occurs for traditional interfacial mechanisms.[15] The experimental finite retention time may come from rich-phase detachment from electrodes due to material heterogeneity, surface wetting, or thermal fluctuation. This can be (partially) avoided by surface processing and scale-down, which should also help increase recyclability and reduce stochasticity. Finally, scale-down should be the primary way to reduce power consumption. More discussion can be found in the SI.

https://doi.org/10.1021/acs.nanolett.2c01765
Nano Lett. XXXX, XXX, XXX−XXX

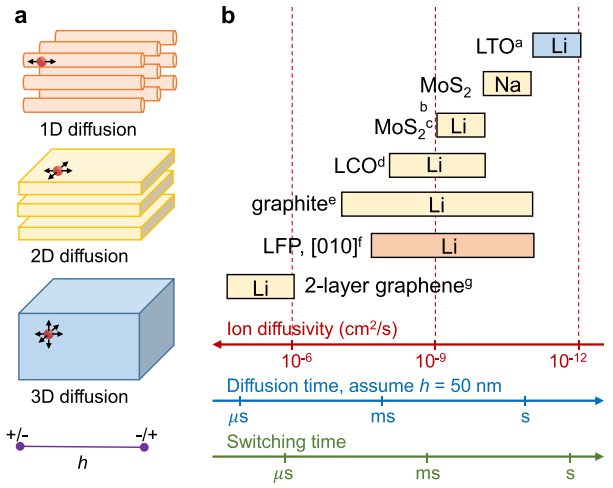

Figure 5. Scales of ion diffusivity (at room temperature), diffusion time, and switching time by multiphase polarization, for several ion-intercalation materials. We assume the length scale between electrodes (h) to be 50 nm to calculate the diffusion time, and we estimate the switching time to be one-tenth of the diffusion time at certain current. The colors labeling diffusion path dimensions in (a) are consistent with the colors for different materials in (b). References (superscript letters): (*a*) ref 19, (*b*) ref 93, (*c*) refs94 and 95, (*d*) ref 96, (*e*) ref 19, (*f*) ref 92, and (*g*) ref 98.

CONCLUSION

In this work, we have proposed and modeled a new interfacial resistive-switching mechanism, multiphase polarization, for a system composed of a multiphase, ion-intercalation nanofilm sandwiched by two ion-blocking electrodes. This model is the first to qualitatively explain the complex RS dynamics of LTO memristors, and it provides insights for device optimization and new designs. Future theoretical work could account for 2D or 3D phase nucleation at interfaces,[56,99] thermal and mechanical effects,[55,57] and multistage phase separation.[58]

ASSOCIATED CONTENT

Supporting Information

The Supporting Information is available free of charge at https://pubs.acs.org/doi/10.1021/acs.nanolett.2c01765.

Details on the dielectric breakdown model; temperature effect; thermal stability analysis; derivation of the generalized Butler–Volmer equation, threshold current, and resistance ratio; parameters; numerical method; additional discussion (PDF)

AUTHOR INFORMATION

Corresponding Author

Martin Z. Bazant − *Department of Chemical Engineering, Massachusetts Institute of Technology, Cambridge, Massachusetts 02139, United States; Department of Mathematics, Massachusetts Institute of Technology, Cambridge, Massachusetts 02139, United States;* orcid.org/0000-0002-8200-4501; Email: bazant@mit.edu

Author

Huanhuan Tian − *Department of Chemical Engineering, Massachusetts Institute of Technology, Cambridge, Massachusetts 02139, United States;* orcid.org/0000-0001-5515-9105

Complete contact information is available at: https://pubs.acs.org/10.1021/acs.nanolett.2c01765

Notes

The authors declare no competing financial interest.

ACKNOWLEDGMENTS

This work was supported by a grant from Ericsson. The authors would like to thank Danniel Cogswell, Willis O'Leary, Dimitrios Fraggedakis, Moran Balaish, Drew Buzzell, Jennifer Rupp, Ju Li, and Pedro de Souza for helpful discussions.

REFERENCES

(1) Waser, R.; Dittmann, R.; Staikov, C.; Szot, K. Redox-based resistive switching memories nanoionic mechanisms, prospects, and challenges. *Adv. Mater.* **2009**, *21*, 2632−2663.
(2) Jeong, D. S.; Thomas, R.; Katiyar, R. S.; Scott, J. F.; Kohlstedt, H.; Petraru, A.; Hwang, C. S. Emerging memories: Resistive switching mechanisms and current status. *Rep. Prog. Phys.* **2012**, *75*, 076502.
(3) Ielmini, D.; Wong, H. S. In-memory computing with resistive switching devices. *Nature Electronics* **2018**, *1*, 333−343.
(4) Waser, R.; Dittmann, R.; Menzel, S.; Noll, T. Introduction to new memory paradigms: Memristive phenomena and neuromorphic applications. *Faraday Discuss.* **2019**, *213*, 11−27.
(5) Li, Y.; Ang, K.-W. Hardware Implementation of Neuromorphic Computing Using Large-Scale Memristor Crossbar Arrays. *Advanced Intelligent Systems* **2021**, *3*, 2000137.
(6) Zidan, M. A.; Strachan, J. P.; Lu, W. D. The future of electronics based on memristive systems. *Nature Electronics* **2018**, *1*, 22−29.
(7) Sawa, A. Resistive switching in transition metal oxides. *Mater. Today* **2008**, *11*, 28−36.
(8) Valov, I.; Waser, R.; Jameson, J. R.; Kozicki, M. N. Electrochemical metallization memories - Fundamentals, applications, prospects. *Nanotechnology* **2011**, *22*, 254003.
(9) Ielmini, D. Resistive switching memories based on metal oxides: Mechanisms, reliability and scaling. *Semicond. Sci. Technol.* **2016**, *31*, 063002.
(10) Wang, Z.; Wu, H.; Burr, G. W.; Hwang, C. S.; Wang, K. L.; Xia, Q.; Yang, J. J. Resistive switching materials forinformation processing. *Nature Reviews Materials* **2020**, *5*, 173−195.
(11) Del Valle, J.; Ramírez, J. G.; Rozenberg, M. J.; Schuller, I. K. Challenges in materials and devices for resistive-switching-based neuromorphic computing. *J. Appl. Phys.* **2018**, *124*, 211101.
(12) Ding, K.; Wang, J.; Zhou, Y.; Tian, H.; Lu, L. L.; Mazzarello, R.; Jia, C.; Zhang, W.; Rao, F.; Ma, E. Phase-change heterostructure enables ultralow noise and drift for memory operation. *Science* **2019**, *366*, 210−215.
(13) Wong, H. S.; Raoux, S.; Kim, S.; Liang, J.; Reifenberg, J. P.; Rajendran, B.; Asheghi, M.; Goodson, K. E. Phase change memory. *Proceedings of the IEEE* **2010**, *98*, 2201−2227.
(14) Zhang, K.; Wang, J.; Huang, Y.; Chen, L. Q.; Ganesh, P.; Cao, Y. High-throughput phase-field simulations and machine learning of resistive switching in resistive random-access memory. *npj Comput. Mater.* **2020**, *6*, 198.
(15) Sassine, G.; La Barbera, S.; Najjari, N.; Minvielle, M.; Dubourdieu, C.; Alibart, F. Interfacial versus filamentary resistive switching in TiO 2 and HfO 2 devices. *J. Vac. Sci. Technol., B: Nanotechnol. Microelectron.: Mater., Process., Meas., Phenom.* **2016**, *34*, 012202.
(16) Hur, J. H.; Lee, M. J.; Lee, C. B.; Kim, Y. B.; Kim, C. J. Modeling for bipolar resistive memory switching in transition-metal oxides. *Phys. Rev. B* **2010**, *82*, 155321.
(17) Yang, J. J.; Pickett, M. D.; Li, X.; Ohlberg, D. A.; Stewart, D. R.; Williams, R. S. Memristive switching mechanism for metal/oxide/metal nanodevices. *Nat. Nanotechnol.* **2008**, *3*, 429−433.
(18) Solanki, A.; Guerrero, A.; Zhang, Q.; Bisquert, J.; Sum, T. C. Interfacial Mechanism for Efficient Resistive Switching in Rud-

dlesden-Popper Perovskites for Non-volatile Memories. *J. Phys. Chem. Lett.* **2020**, *11*, 463−470.
(19) Nitta, N.; Wu, F.; Lee, J. T.; Yushin, G. Li-ion battery materials. *Mater. Today* **2015**, *18*, 252−264.
(20) Stark, M. S.; Kuntz, K. L.; Martens, S. J.; Warren, S. C. Intercalation of Layered Materials from Bulk to 2D. *Adv. Mater.* **2019**, *31*, 1808213.
(21) Zhou, J.; Lin, Z.; Ren, H.; Duan, X.; Shakir, I.; Huang, Y.; Duan, X. Layered Intercalation Materials. *Adv. Mater.* **2021**, *33*, 2004557.
(22) Riess, I. Electrochemistry of mixed ionic-electronic conductors. *CRC Handb. Solid State Electrochem.* **1997**, 223−268.
(23) Bazant, M. Z. Theory of chemical kinetics and charge transfer based on nonequilibrium thermodynamics. *Acc. Chem. Res.* **2013**, *46*, 1144−1160.
(24) Morgan, B. J.; Carrasco, J.; Teobaldi, G. Variation in surface energy and reduction drive of a metal oxide lithium-ion anode with stoichiometry: A DFT study of lithium titanate spinel surfaces. *Journal of Materials Chemistry A* **2016**, *4*, 17180−17192.
(25) Liu, Y.; Lian, J.; Sun, Z.; Zhao, M.; Shi, Y.; Song, H. The first-principles study for the novel optical properties of LiTi2O4, Li4Ti5O12, Li2Ti2O4 and Li7Ti5O12. *Chem. Phys. Lett.* **2017**, *677*, 114−119.
(26) Yao, X.; Klyukin, K.; Lu, W.; Onen, M.; Ryu, S.; Kim, D.; Emond, N.; Waluyo, I.; Hunt, A.; del Alamo, J. A.; Li, J.; Yildiz, B. Protonic solid-state electrochemical synapse for physical neural networks. *Nat. Commun.* **2020**, *11*, 3134.
(27) Gellings, P. J., Bouwmeester, H., Eds. *The CRC Handbook of Solid State Electrochemistry*; CRC Press, 1997.
(28) Cox, P. A. *Transition metal oxides: an introduction to their electronic structure and properties*; Oxford University Press, 2010; Vol. *27*.
(29) Nguyen, V. S.; et al. Direct Evidence of Lithium Ion Migration in Resistive Switching of Lithium Cobalt Oxide Nanobatteries. *Small* **2018**, *14*, 1801038.
(30) Sharbati, M. T.; Du, Y.; Torres, J.; Ardolino, N. D.; Yun, M.; Xiong, F. Low-Power, Electrochemically Tunable Graphene Synapses for Neuromorphic Computing. *Adv. Mater.* **2018**, *30*, 1802353.
(31) Fuller, E. J.; Gabaly, F. E.; Léonard, F.; Agarwal, S.; Plimpton, S. J.; Jacobs-Gedrim, R. B.; James, C. D.; Marinella, M. J.; Talin, A. A. Li-Ion Synaptic Transistor for Low Power Analog Computing. *Adv. Mater.* **2017**, *29*, 1604310.
(32) Onen, M.; Emond, N.; Li, J.; Yildiz, B.; Del Alamo, J. A. CMOS-Compatible Protonic Programmable Resistor Based on Phosphosilicate Glass Electrolyte for Analog Deep Learning. *Nano Lett.* **2021**, *21*, 6111−6116.
(33) Gonzalez-Rosillo, J. C.; Balaish, M.; Hood, Z. D.; Nadkarni, N.; Fraggedakis, D.; Kim, K. J.; Mullin, K. M.; Pfenninger, R.; Bazant, M. Z.; Rupp, J. L. Lithium-Battery Anode Gains Additional Functionality for Neuromorphic Computing through Metal-Insulator Phase Separation. *Adv. Mater.* **2020**, *32*, 1907465.
(34) Zhao, B.; Ran, R.; Liu, M.; Shao, Z. A comprehensive review of Li 4 Ti 5 O 12 -based electrodes for lithium-ion batteries: The latest advancements and future perspectives. *Mater. Sci. Eng. R* **2015**, *98*, 1−71.
(35) Fraggedakis, D.; Mirzadeh, M.; Zhou, T.; Bazant, M. Z. Dielectric Breakdown by Electric-field Induced Phase Separation. *J. Electrochem. Soc.* **2020**, *167*, 113504.
(36) Young, D.; Ransil, A.; Amin, R.; Li, Z.; Chiang, Y. M. Electronic conductivity in the Li4/3Ti5/3O 4-Li7/3Ti5/3O4 system and variation with state-of-charge as a Li battery anode. *Adv. Energy Mater.* **2013**, *3*, 1125−1129.
(37) Scharner, S.; Weppner, W.; Schmid-Beurmann, P. Evidence of Two-Phase Formation upon Lithium Insertion into the Li1.33Ti1.67 O 4 Spinel. *J. Electrochem. Soc.* **1999**, *146*, 857−861.
(38) Sze, S. M., Ng, K. K. *Physics of Semiconductor Devices*; John Wiley & Sons, 2007.
(39) Mani, A.; Zangle, T. A.; Santiago, J. G. On the Propagation of Concentration Polarization from Microchannel-Nanochannel Interfaces Part I: Analytical Model and Characteristic Analysis. *Langmuir* **2009**, *25*, 3898−3908.
(40) Zangle, T. A.; Mani, A.; Santiago, J. G. On the Propagation of Concentration Polarization from Microchannel-Nanochannel interfaces Part II: Numerical and experimental study. *Langmuir* **2009**, *25*, 3909−3916.
(41) Dydek, E. V.; Zaltzman, B.; Rubinstein, I.; Deng, D. S.; Mani, A.; Bazant, M. Z. Overlimiting current in a microchannel. *Phys. Rev. Lett.* **2011**, *107*, 118301.
(42) Dydek, E. V.; Bazant, M. Z. Nonlinear dynamics of ion concentration polarization in porous media: The leaky membrane model. *AIChE J.* **2013**, *59*, 3539−3555.
(43) Nielsen, C. P.; Bruus, H. Concentration polarization, surface currents, and bulk advection in a microchannel. *Phys. Rev. E* **2014**, *90*, 043020.
(44) Mishchuk, N. A. Concentration polarization of interface and non-linear electrokinetic phenomena. *Adv. Colloid Interface Sci.* **2010**, *160*, 16−39.
(45) Andersen, M. B.; Van Soestbergen, M.; Mani, A.; Bruus, H.; Biesheuvel, P. M.; Bazant, M. Z. Current-induced membrane discharge. *Phys. Rev. Lett.* **2012**, *109*, 108301.
(46) Schlumpberger, S.; Lu, N. B.; Suss, M. E.; Bazant, M. Z. Scalable and Continuous Water Deionization by Shock Electrodialysis. *Environmental Science and Technology Letters* **2015**, *2*, 367−372.
(47) Mani, A.; Bazant, M. Z. Deionization shocks in microstructures. *Phys. Rev. E* **2011**, *84*, 061504.
(48) Tian, H.; Alkhadra, M. A.; Bazant, M. Z. Theory of shock electrodialysis I: Water dissociation and electrosmotic vortices. *J. Colloid Interface Sci.* **2021**, *589*, 605−615.
(49) Tian, H.; Alkhadra, M. A.; Bazant, M. Z. Theory of shock electrodialysis II: Mechanisms of selective ion removal. *J. Colloid Interface Sci.* **2021**, *589*, 616−621.
(50) Tian, H.; Alkhadra, M. A.; Conforti, K. M.; Bazant, M. Z. Continuous and Selective Removal of Lead from Drinking Water by Shock Electrodialysis. *ACS ES&T Water* **2021**, *1*, 2269−2274.
(51) Smith, R. B.; Bazant, M. Z. Multiphase Porous Electrode Theory. *J. Electrochem. Soc.* **2017**, *164*, E3291−E3310.
(52) Singh, G. K.; Ceder, G.; Bazant, M. Z. Intercalation dynamics in rechargeable battery materials: General theory and phase-transformation waves in LiFePO4. *Electrochim. Acta* **2008**, *53*, 7599−7613.
(53) Tang, M.; Huang, H.-Y.; Meethong, N.; Kao, Y.-H.; Carter, W. C.; Chiang, Y.-M. Model for the particle size, overpotential, and strain dependence of phase transition pathways in storage electrodes: application to nanoscale olivines. *Chem. Mater.* **2009**, *21*, 1557−1571.
(54) Bai, P.; Cogswell, D. A.; Bazant, M. Z. Suppression of phase separation in LiFePO4 nanoparticles during battery discharge. *Nano Lett.* **2011**, *11*, 4890−4896.
(55) Cogswell, D. A.; Bazant, M. Z. Coherency Strain and the Kinetics of Phase Separation in {L}i{F}e{PO}$_4$ Nanoparticles. *ACS Nano* **2012**, *6*, 2215−2225.
(56) Cogswell, D. A.; Bazant, M. Z. Theory of coherent nucleation in phase-separating nanoparticles. *Nano Lett.* **2013**, *13*, 3036−3041.
(57) Nadkarni, N.; Rejovitsky, E.; Fraggedakis, D.; Di Leo, C. V.; Smith, R. B.; Bai, P.; Bazant, M. Z. Interplay of phase boundary anisotropy and electro-auto-catalytic surface reactions on the lithium intercalation dynamics in LiXFePO4 plateletlike nanoparticles. *Phys. Rev. Mater.* **2018**, *2*, 085406.
(58) Smith, R. B.; Khoo, E.; Bazant, M. Z. Intercalation kinetics in multiphase-layered materials. *J. Phys. Chem. C* **2017**, *121*, 12505−12523.
(59) Nadkarni, N.; Zhou, T.; Fraggedakis, D.; Gao, T.; Bazant, M. Z. Modeling the Metal-Insulator Phase Transition in LixCoO2 for Energy and Information Storage. *Adv. Funct. Mater.* **2019**, *29*, 1902821.
(60) De Klerk, N. J.; Vasileiadis, A.; Smith, R. B.; Bazant, M. Z.; Wagemaker, M. Explaining key properties of lithiation in TiO2 -anatase Li-ion battery electrodes using phase-field modeling. *Phys. Rev. Mater.* **2017**, *1*, 025404.

https://doi.org/10.1021/acs.nanolett.2c01765
Nano Lett. XXXX, XXX, XXX−XXX

(61) Bosman, A. J.; van Daal, H. J. Small-polaron versus band conduction in some transition-metal oxides. *Adv. Phys.* **1970**, *19*, 1−117.
(62) Ellis, B.; Perry, L. K.; Ryan, D. H.; Nazar, L. F. Small polaron hopping in LixFePO4 solid solutions: Coupled lithium-ion and electron mobility. *J. Am. Chem. Soc.* **2006**, *128*, 11416−11422.
(63) Zhou, F.; Maxisch, T.; Ceder, G. Configurational electronic entropy and the phase diagram of mixed-valence oxides: The case of LixFePO4. *Phys. Rev. Lett.* **2006**, *97*, 155704.
(64) Mikkelsen, K. V.; Ratner, M. A. Electron Tunneling in Solid-State Electron-Transfer Reactions. *Chem. Rev.* **1987**, *87*, 113−153.
(65) Sood, A.; Poletayev, A. D.; Cogswell, D. A.; Csernica, P. M.; Mefford, J. T.; Fraggedakis, D.; Toney, M. F.; Lindenberg, A. M.; Bazant, M. Z.; Chueh, W. C. Electrochemical ion insertion from the atomic to the device scale. *Nature Reviews Materials* **2021**, *6*, 847−867.
(66) Mebane, D. S.; De Souza, R. A. A generalised space-charge theory for extended defects in oxygen-ion conducting electrolytes: from dilute to concentrated solid solutions. *Energy Environ. Sci.* **2015**, *8*, 2935−2940.
(67) Guyer, J. E.; Boettinger, W. J.; Warren, J. A.; McFadden, G. B. Phase field modeling of electrochemistry. I. Equilibrium. *Phys. Rev. E* **2004**, *69*, 021603.
(68) Guyer, J. E.; Boettinger, W. J.; Warren, J. A.; McFadden, G. B. Phase field modeling of electrochemistry. II. Kinetics. *Phys. Rev. E* **2004**, *69*, 021604.
(69) Cahn, J. W.; Hilliard, J. E. Free energy of a nonuniform system. I. Interfacial free energy. *J. Chem. Phys.* **1958**, *28*, 258−267.
(70) Zhao, H.; Storey, B. D.; Braatz, R. D.; Bazant, M. Z. Learning the Physics of Pattern Formation from Images. *Phys. Rev. Lett.* **2020**, *124*, 060201.
(71) Maier, J. *Physical Chemistry of Ionic Materials: Ions and Electrons in Solids*; John Wiley & Sons, 2004.
(72) Menzel, S.; Von Witzleben, M.; Havel, V.; Böttger, U. The ultimate switching speed limit of redox-based resistive switching devices. *Faraday Discuss.* **2019**, *213*, 197−213.
(73) Tung, R. T. The physics and chemistry of the Schottky barrier height. *Appl. Phys. Rev.* **2014**, *1*, 011304.
(74) Cowley, A. M.; Sze, S. M. Surface states and barrier height of metal-semiconductor systems. *J. Appl. Phys.* **1965**, *36*, 3212−3220.
(75) Bai, P.; Bazant, M. Z. Charge transfer kinetics at the solid-solid interface in porous electrodes. *Nat. Commun.* **2014**, *5*, 3585.
(76) Marcus, R. A. Chemical and electrochemical electron-transfer theory. *Annu. Rev. Phys. Chem.* **1964**, *15*, 155.
(77) Marcus, R. A. On the Theory of Electron-Transfer Reactions. VI. Unified Treatment for Homogeneous and Electrode Reactions. *J. Chem. Phys.* **1965**, *43*, 679−701.
(78) Marcus, R. A.; Sutin, N. Electron transfers in chemistry and biology. *Biochim. Biophys. Acta* **1985**, *811*, 265−322.
(79) Marcus, R. A. Electron Transfer Reactions in Chemistry: Theory and Experiment. *Rev. Mod. Phys.* **1993**, *65*, 599−610.
(80) Chidsey, C. E. Free energy and temperature dependence of electron transfer at the metal-electrolyte interface. *Science* **1991**, *251*, 919−922.
(81) Henstridge, M. C.; Laborda, E.; Rees, N. V.; Compton, R. G. Marcus-Hush-Chidsey theory of electron transfer applied to voltammetry: A review. *Electrochim. Acta* **2012**, *84*, 12−20.
(82) Laborda, E.; Henstridge, M. C.; Compton, R. G. Asymmetric Marcus theory: Application to electrode kinetics. *J. Electroanal. Chem.* **2012**, *667*, 48−53.
(83) Laborda, E.; Henstridge, M. C.; Batchelor-Mc Auley, C.; Compton, R. G. Asymmetric marcus-Hush theory for voltammetry. *Chem. Soc. Rev.* **2013**, *42*, 4894−4905.
(84) Zeng, Y.; Bai, P.; Smith, R. B.; Bazant, M. Z. Simple formula for asymmetric Marcus-Hush kinetics. *J. Electroanal. Chem.* **2015**, *748*, 52−57.
(85) Fletcher, S. The theory of electron transfer. *J. Solid State Electrochem.* **2010**, *14*, 705−739.
(86) Fraggedakis, D.; McEldrew, M.; Smith, R. B.; Krishnan, Y.; Zhang, Y.; Bai, P.; Chueh, W. C.; Shao-Horn, Y.; Bazant, M. Z. Theory of coupled ion-electron transfer kinetics. *Electrochim. Acta* **2021**, *367*, 137432.
(87) Lien, C. D.; So, F. C.; Nicolet, M. A. An Improved Forward I-V Method For Nonideal Schottky Diodes With High Series Resistance. *IEEE Trans. Electron Devices* **1984**, *31*, 1502−1503.
(88) Aubry, V.; Meyer, F. Schottky diodes with high series resistance: Limitations of forward I-V methods. *J. Appl. Phys.* **1994**, *76*, 7973−7984.
(89) Takami, N.; Hoshina, K.; Inagaki, H. Lithium Diffusion in Li4/3Ti5/3O4 Particles during Insertion and Extraction. *J. Electrochem. Soc.* **2011**, *158*, A725.
(90) Wagemaker, M.; Van Eck, E. R.; Kentgens, A. P.; Mulder, F. M. Li-ion diffusion in the equilibrium nanomorphology of spinel Li 4+xTi5O12. *J. Phys. Chem. B* **2009**, *113*, 224−230.
(91) Prezioso, M.; Merrikh-Bayat, F.; Hoskins, B. D.; Adam, G. C.; Likharev, K. K.; Strukov, D. B. Training and operation of an integrated neuromorphic network based on metal-oxide memristors. *Nature* **2015**, *521*, 61−64.
(92) Malik, R.; Burch, D.; Bazant, M.; Ceder, G. Particle size dependence of the ionic diffusivity. *Nano Lett.* **2010**, *10*, 4123−4127.
(93) Li, Y.; Liang, Y.; Robles Hernandez, F. C.; Deog Yoo, H.; An, Q.; Yao, Y. Enhancing sodium-ion battery performance with interlayer-expanded MoS2-PEO nanocomposites. *Nano Energy* **2015**, *15*, 453−461.
(94) Hu, Z.; Liu, Q.; Sun, W.; Li, W.; Tao, Z.; Chou, S. L.; Chen, J.; Dou, S. X. MoS2 with an intercalation reaction as a long-life anode material for lithium ion batteries. *Inorganic Chemistry Frontiers* **2016**, *3*, 532−535.
(95) Santa-Ana, M. A.; Sanchez, V.; Gonzalez, G. Temperature effects on the diffusion of lithium in MoS2. *Electrochim. Acta* **1995**, *40*, 1773−1775.
(96) Park, M.; Zhang, X.; Chung, M.; Less, G. B.; Sastry, A. M. A review of conduction phenomena in Li-ion batteries. *J. Power Sources* **2010**, *195*, 7904−7929.
(97) Li, Y.; Lu, Y.; Adelhelm, P.; Titirici, M. M.; Hu, Y. S. Intercalation chemistry of graphite: Alkali metal ions and beyond. *Chem. Soc. Rev.* **2019**, *48*, 4655−4687.
(98) Kühne, M.; Paolucci, F.; Popovic, J.; Ostrovsky, P. M.; Maier, J.; Smet, J. H. Ultrafast lithium diffusion in bilayer graphene. *Nat. Nanotechnol.* **2017**, *12*, 895−900.
(99) Gránásy, L.; Pusztai, T.; Saylor, D.; Warren, J. A. Phase field theory of heterogeneous crystal nucleation. *Phys. Rev. Lett.* **2007**, *98*, 035703.

https://doi.org/10.1021/acs.nanolett.2c01765
Nano Lett. XXXX, XXX, XXX−XXX